THE JOURNAL OF PHYSICAL CHEMISTRY C

Article

pubs.acs.org/JPCC

In- and Out-Dependent Interactions of Iron with Carbon Nanotubes

Liang Yu,[†] Wei-Xue Li,*[,†,‡] Xiulian Pan,*[,†] and Xinhe Bao[†]

[†]State Key Laboratory of Catalysis and [‡]Center for Theoretical and Computational Chemistry, Dalian Institute of Chemical Physics, Chinese Academy of Sciences, Dalian 116023, China

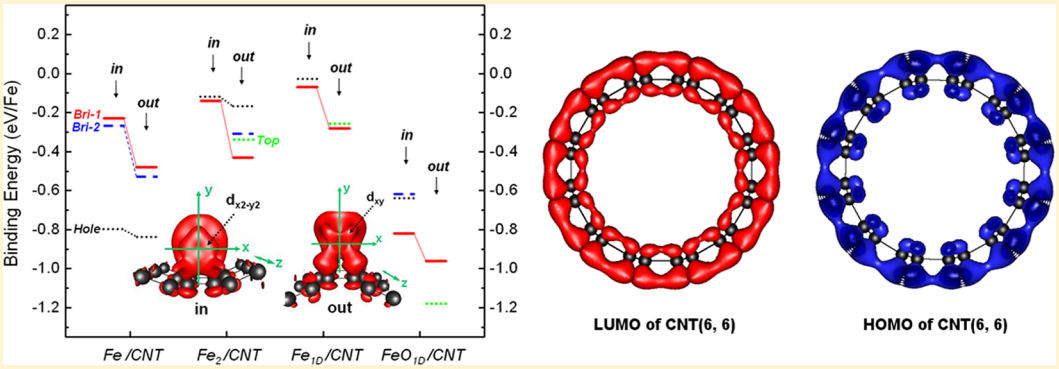

ABSTRACT: The interaction of an Fe atom, an Fe dimer, a one-dimensional Fe nanowire, and an FeO nanowire with a single-walled armchair carbon nanotube (CNT) (8, 8) is investigated using density functional theory calculations. The results show that for all iron species the bonding with the outside wall of the CNT is stronger than that with the inside wall. Analysis of the electron distribution of the CNT shows that the curvature of the CNT induces a significant electron disparity at the inside and outside regions and more electrons are distributed on the outer surface. The properties of the frontier orbitals of the CNT are studied, and the results show that the highest occupied molecular orbital and lowest unoccupied molecular orbital are mainly located outside the tube, which may account for the in- and out-dependent interactions of Fe species with the CNT surface and hence different chemical reactivities of CNT-loaded metals.

1. INTRODUCTION

Carbon nanotubes (CNTs) can be considered as graphene layers which roll up, forming coaxial columns. The curvature of the carbon network alters the hybridization of electronic orbitals, which deforms the pure sp^2 hybridization of graphene with a sp^3 character, inducing different chemical environments in the cavity and on the outer surface.[1,2] Modified properties of metal/metal oxide nanoparticles/clusters in the cavity with respect to those dispersed on the outer surface have been frequently observed, although the exact influence of this electronic structure is not elucidated yet.[3−6] For example, iron oxide and ruthenium oxide nanoparticles confined inside the tube can be reduced more facilely than those residing on the outer wall.[3,7] The Rh nanoparticles confined inside the CNT exhibit better catalytic activity and selectivity for the conversion of CO and H_2 to ethanol compared to outside-dispersed particles.[6] Cinchonidine-modified Pt clusters were shown with a better activity and enantioselectivity for hydrogenation of α-ketoesters when encapsulated within CNTs.[8]

In addition to the different adsorption and diffusion of molecules inside the CNT channels[9] and the restriction of the size-limited channels on the particle size growth,[4,5] the interactions of the CNT walls with the metal species may also play an important role yet to be elucidated in depth. Metal atoms and dimers have been widely used as probes to investigate the interaction of a CNT with loaded clusters, which to some extent provides preliminary insights into the metal/CNT interaction system.[10−13] Vo et al. studied single Fe atom adsorption on a single-walled carbon nanotube (SWCNT) and found that the stability, band gap, and total magnetic moment of the systems depend on the location of the Fe atom relative to the carbon nanotube surface.[10] Yagi et al. reported different adsorption strengths for 3d transition-metal atoms and dimers on the inside and outside of an SWCNT by first-principles density functional calculations.[11] However, interaction of larger aggregates with a CNT has not yet been studied to approach the experimental applications. Furthermore, the origin of this inside−outside difference is yet to be clarified.

To shed light on these questions, iron as a typical transition metal is taken as a probe and studied by density functional theory calculations. A series of aggregates ranging from a single atom to a one-dimensional nanowire are adopted to investigate the interaction of iron with a CNT and its dependence on the size of the models, including a single Fe atom, an Fe dimer, and an Fe nanowire. Since iron is highly active and prone to be oxidized under realistic conditions, understanding the inter-

Received: March 9, 2012
Revised: June 24, 2012
Published: July 13, 2012

action between the oxidized iron and the CNTs is valuable and studied by the FeO nanowire. The interaction mechanism and electronic structures of CNTs are analyzed, aiming to elucidate the inside- and outside-dependent properties of metal aggregates. Understanding the trend may provide valuable insights into the interaction of even larger aggregates, for instance, metal nanoparticles with CNTs.

2. COMPUTATIONAL DETAILS

All calculations in this work were performed using the Vienna Ab-initio Simulation Package (VASP) with the projector-augmented wave method and a cutoff energy of 400 eV.[14−18] The PW91 functional with generalized gradient approximation method was adopted for the exchange-correlation term.[19] The structure was fully relaxed using the conjugated gradient method until the force on each atom was less than 0.05 eV/Å. The Monkhorst−Pack scheme was used to sample the Brillouin zone.[20]

Models of an iron atom (Fe), an iron dimer (Fe_2), a one-dimensional iron nanowire (Fe_{1D}), and an iron oxide nanowire (FeO_{1D}) on an SWCNT (8, 8) were used. Four adsorption sites were considered: hole, top, bridge-1, and bridge-2 (Figure 1). Figure 2 shows the schematic structures of iron species

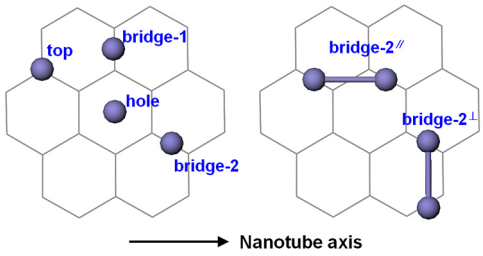

Figure 1. Adsorption sites on an SWCNT. The right panel shows two different configurations for the adsorption of an Fe dimer on the bridge-2 site.

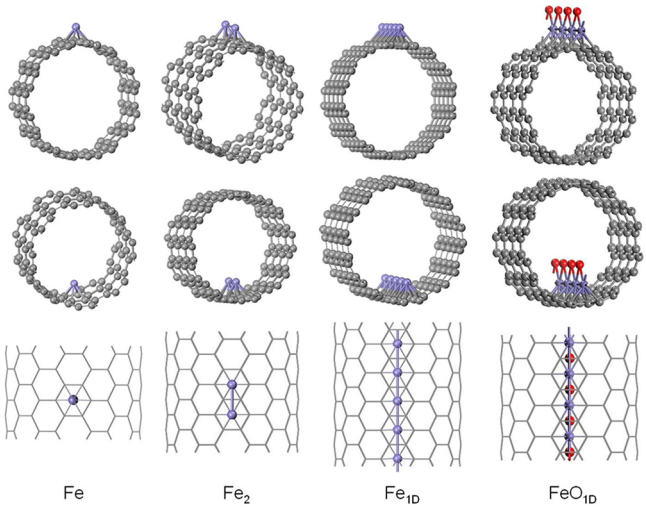

Figure 2. Optimized structures of Fe, Fe_2, Fe_{1D}, and FeO_{1D} adsorbed on the outer (top panel) and inner (middle panle) hole sites of an (8, 8) SWCNT. The bottom panel shows their top view.

adsorbed on the hole site. A periodically repeating tetragonal supercell was utilized with lattice constants $a = b = 26$ Å. For the Fe atom (Fe/CNT) and dimer (Fe_2/CNT) in the c direction, the supercells consisted of three (7.379 Å) and four (9.838 Å) unit cells of the bare tube, respectively. For the one-dimensional nanowire models (Fe_{1D}/CNT and FeO_{1D}/CNT), we used the unit c vector of the bare tube (2.46 Å) with one Fe or FeO per unit cell. The optimized structures of Fe_{1D}/CNT and FeO_{1D}/CNT are shown in Figure 2. The isolated Fe dimer was calculated in a large rectangular supercell (12.1 × 12.2 × 12.3 Å) and structurally optimized. The isolated Fe_{1D} and FeO_{1D} were calculated in the same supercell as Fe_{1D}/CNT and FeO_{1D}/CNT and structurally optimized. A 1 × 1 × 8 k-point mesh sampling was used for Fe/CNT, 1 × 1 × 4 for Fe_2/CNT, and 1 × 1 × 11 for Fe_{1D}/CNT and FeO_{1D}/CNT. Spin polarization was considered in all calculations, and the electronic structures with converged magnetic moments of iron were optimized to the ground state.

The binding energies, magnetic moments, and bonding lengths are listed in Table 1. The binding energies for the iron/CNT interaction structures are defined as $E_b = (E_{ads/CNT} - E_{CNT} - E_{ads})/n$, where $E_{ads/CNT}$ is the total energy of the adsorbed structure, E_{CNT} is the energy of the pristine CNT, E_{ads} is the energy of isolated iron aggregates, and n is the number of Fe atoms per unit cell.

3. RESULTS AND DISCUSSION

3.1. Interaction of Iron Species with SWCNT (8, 8).

3.1.1. Interaction of an Fe Atom with the CNT (Fe/CNT). For the interaction of an Fe atom with the CNT on the same site, the outer adsorptions are more stable than the corresponding inner ones, indicating that the Fe atom bonds more strongly with the outer surface of the CNT. One also sees that the adsorption on the hole site is the most stable among all sites for both inner and outer cases, which is consistent with the more quenched magnetic moment (μ) of hole-site adsorption (2 μ_B) compared with that of the other sites (4 μ_B); this is also reflected by the shorter Fe−C bonds (2.04−2.09 Å) on the hole site than those (2.15−2.29 Å) on the other sites. However, the binding energy (−0.84 eV) on the outer hole site is only slightly higher than that on the inner hole site (−0.80 eV). This is likely attributed to the different bonding features of the Fe atom on the inner and outer hole sites. As shown in Table 1, six short bonds (2.04−2.11 Å) form at the inner hole site, while at the outer hole site only four short bonds (2.09 Å) form, with the other two elongated to 2.20 Å, which offsets to an extent the difference in bonding strength between inner and outer adsorptions. The finding of favored adsorption of the Fe atom on the outer surface of the CNT is consistent with previous calculations on different SWCNTs.[10−12] Compared with the results of the (8, 0) tube used in earlier studies in which the binding energy difference between inner and outer hole-site adsorptions is 0.33 eV,[10,12] this difference for (8, 8) here (0.04 eV) is smaller. This is probably due to the large curvature effect for the smaller diameter (6.3 Å) of the (8, 0) SWCNT than that (10.9 Å) of the (8, 8) SWCNT.

3.1.2. Interaction of Fe_2 with the CNT (Fe_2/CNT). Fe_2 dimers on inner bridge-2$^{\parallel}$ (Bri-2$^{\parallel}$) and top sites move to the bridge-1 (Bri-1) site after structural optimization. The 2-fold-coordinated bridge site becomes more favored for both inner and outer adsorptions in contrast to the 6-fold-coordinated hole site for a single Fe atom. Moreover, the binding of Fe_2 with the CNT on all sites is weaker than that in Fe/CNT because of the stabilization from Fe−Fe bonding in the dimer. The overall energy gain (per Fe atom) with respect to the isolated Fe atoms can be defined by $E_b' = (E_{ads/CNT} - E_{CNT})/n - E_{Fe\ atom}$, where $E_{Fe\ atom}$ is the total energy of an isolated Fe

dx.doi.org/10.1021/jp302311r | J. Phys. Chem. C 2012, 116, 16461−16466

Table 1. Binding Energies, Magnetic Moments (μ), and Lengths of Fe−C and Fe−Fe Bonds of Fe/CNT, Fe_2/CNT, Fe_{1D}/CNT, and FeO_{1D}/CNT

	adsorption site	E_b (eV/Fe)	E_b' (eV/Fe)	μ (μ_B/Fe)	Fe−C length[a] (Å)	Fe−Fe length (Å)
Fe/CNT	inner hole	−0.80		2	2.04 (2), 2.11 (4)	
	Bri-1	−0.23		4	2.29, 2.25	
	Bri-2	−0.27		4	2.28, 2.29	
	outer hole	−0.84		2	2.20 (2), 2.09 (4)	
	Bri-1	−0.48		4	2.18, 2.17	
	Bri-2	−0.53		4	2.15, 2.16	
Fe_2/CNT	inner hole	−0.12	−1.46	3.25	2.24 (2), 2.23 (2)	2.19
	Bri-1	−0.14	−1.48	3.13	2.16 (2), 2.17 (2)	2.10
	Bri-2$^{\perp}$	−0.25	−1.59	3.15	2.22, 2.24, 2.34, 2.37	2.17
	outer hole	−0.17	−1.51	3.30	2.34 (2), 2.40 (2)	2.16
	Bri-1	−0.43	−1.77	3.03	2.10 (2), 2.11 (2)	2.15
	Bri-2$^{\parallel}$	−0.31	−1.65	3.02	2.28, 2.26, 2.17, 2.14	2.09
	Bri-2$^{\perp}$	−0.43	−1.77	3.03	2.07, 2.10, 2.14, 2.16	2.11
	top	−0.34	−1.68	3.01	2.05, 2.07, 2.31	2.10
Fe_{1D}/CNT	inner hole	−0.03	−1.68	3.02	2.26 (2), 2.32 (2)	2.46
	Bri-1	−0.07	−1.72	2.97	2.14 (2)	2.46
	outer Bri-1	−0.28	−1.93	3.09	2.00 (2)	2.46
	top	−0.26	−1.91	3.02	2.06	2.46
FeO_{1D}/CNT	inner hole	−0.64		0.63	2.15 (2), 2.28 (2), 2.29(2)	2.46 (1.75[b])
	Bri-1	−0.82		2.00	2.13 (2), 2.14 (2)	2.46 (1.77[b])
	Bri-2	−0.62		2.42	2.19 (2), 2.20 (2)	2.46 (1.75[b])
	outer Bri-1	−0.96		2.03	2.12, 2.13	2.46 (1.75[b])
	top	−1.18		2.28	2.03	2.46 (1.74[b])

[a]The number of Fe−C bonds with the same length is indicated in parentheses. [b]Length of the Fe−O bond.

atom. E_b' includes both the Fe−Fe and Fe−C interactions, and the results are given in Table 1 too. Compared to E_b for Fe/CNT, the larger energy gain from Fe−Fe bonding is clearly seen. The contribution from Fe−Fe interaction can be measured roughly by the difference between E_b' and E_b ($|E_b' - E_b|$), which is 1.34 eV and significantly larger than the Fe−C interaction energy ($|E_b|$ = 0.12−0.43 eV). Thus, the bonding of Fe−Fe (∼2.15 Å) is more preferred than that of Fe−C, which weakens the interaction of Fe with the CNT surface. The data in Table 1 also suggest that Fe_2 bonds more strongly with the outer sites than with the corresponding inner ones, consistent with an earlier study for Fe, Co, and Ni dimers on a (4, 4) SWCNT.[11]

3.1.3. Interactions of Fe_{1D} and FeO_{1D} Nanowires with the CNT (Fe_{1D}/CNT and FeO_{1D}/CNT). Table 1 shows that E_b of Fe_{1D}/CNT becomes even smaller than that of Fe_2/CNT. Owing to the formation of one more Fe−Fe bond in Fe_{1D}/CNT, a larger difference between E_b' and E_b ($|E_b' - E_b|$ = 1.65 eV) compared with that in Fe_2/CNT indicates an increased contribution from Fe−Fe interaction, although the Fe−Fe bond length is elongated to 2.46 Å from ∼2.15 Å of Fe_2/CNT. The preferred Fe−Fe interaction further weakens the interaction between Fe and the CNT surface. In comparison, the binding energy of the FeO nanowire on the most favored site (−1.18 eV, outer top) is notably larger than that of Fe_{1D} (−0.28 eV, outer Bri-1), indicating that the oxidization of the Fe nanowire enhances its interaction with the CNT and stabilizes the hybrid system. Similar to Fe and Fe_2, both Fe_{1D} and FeO_{1D} bond more strongly with the outer sites with apparently shorter Fe−C bonds than those of the inner ones.

The overview map in Figure 3 shows the following more clearly: (1) All the Fe species bond more strongly with the outer surface of the CNT than with the inner surface. Interestingly, on the Bri-1 site the inside and outside difference

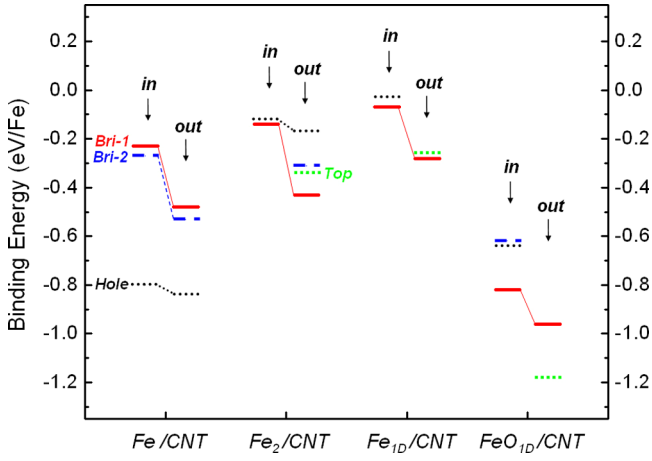

Figure 3. Overview of the binding energies of different Fe species on the inner and outer sites of a CNT.

of E_b changes subtly from the Fe atom (0.25 eV) to Fe_2 (0.29 eV) to Fe_{1D} (0.21 eV), indicating that it is independent of the size of the models. (2) The interaction between Fe and the CNT becomes weaker as Fe grows from one atom to a dimer to a 1D nanowire due to the formation of more preferred Fe−Fe bonds in the system. The most stable adsorption site changes from the 6-fold-coordinated hole site in Fe/CNT to the 2-fold-coordinated Bri-1 site in Fe_{1D}/CNT owing to the more competitive Fe−Fe interaction than Fe−C. This indicates that iron atoms tend to aggregate to bond with each other rather than atomically disperse when loaded on the CNT, as can be seen more clearly from the gradual increase of binding energies from the $|E_b|$ of Fe/CNT to the $|E_b'|$ of Fe_2/CNT and Fe_{1D}/CNT. Yuan et al. also observed that a Fe_4 cluster formed a stable tetrahedral structure rather than a flat quadrangle

dx.doi.org/10.1021/jp302311r | J. Phys. Chem. C 2012, 116, 16461−16466

structure on the CNT.[21] Sun et al. showed that Fe chains did not bond stably with the CNT except for the small-size tubes.[22] The clustering of iron atoms has also been observed experimentally on the surface of highly oriented pyrolitic graphite.[23] Our calculation indicates that the bonding strength of an Fe single atom, dimer, and nanowire with a flat graphene surface lies between those with the inner and outer CNT surfaces, which clearly shows the effect of the CNT's curvature.

Less stable binding of iron species inside the tube could influence the interaction of iron species with other molecules with respect to those on the outside sites. For example, our calculations on the binding energy of CO and O_2 on iron of the Fe_{1D}/CNT model (Table 2) show that both CO and O_2 are adsorbed more strongly on the inner Fe nanowire. The inside−outside E_a difference is 0.17 eV for CO and 0.27 eV for O_2. This indicates that the chemical reactivity of iron can be modulated by the CNT through interaction with its interior and exterior surfaces, providing different catalytic properties when loaded inside and outside the CNT.

Table 2. Binding Energies (eV) of CO and O_2 on an Fe Nanowire inside and outside the CNT[a]

	E_b (CO)	E_b (O_2)
Fe_{1D}-in-Bri-1	−2.43	−2.45
Fe_{1D}-out-Bri-1	−2.26	−2.18

[a]This was calculated in a 1 × 1 × 4 supercell of Fe_{1D}/CNT with a coverage of 1/4 monolayer (one CO or O_2 per four iron atoms). The optimized adsorption sites for CO and O_2 are atop and bridge sites on the iron nanowire, respectively.

Although the iron/CNT systems are generally ferromagnetic with significant magnetic moments, we find that there is little distinct difference in the magnetic moments of inner and outer adsorptions. In contrast, the magnetic moments of Co/CNT and Ni/CNT systems depend not only on the inner or outer adsorption sites but also on the diameter of the nanotube.[11]

3.2. Analysis of the Bonding of Fe_2 with the CNT. To understand the bonding difference on the inner and outer sites, the interaction of Fe_2 with the CNT on the Bri-1 site is investigated. Figure 4a shows the projected density of states (DOS) of the 3d orbitals of Fe_2 on the inner and outer Bri-1 sites. The d_{xy} state is apparently broadened with no sharp peaks, which is quite different from other d states. This is due to the formation of covalent bonding between the d_{xy} orbtial of Fe and the p_y orbital of C. As shown in Figure 4b, the orientation of the d_{xy} orbital of Fe_2 matches well with that of the p_y orbital of C, which favors the bonding between them.

The integral area of each state in Figure 4a can be used as a measure of the amount of electrons on that state. Thus, one sees that the d_{xy} and $d_{x^2-y^2}$ states of the inner case differ significantly from those of the outer case in the amount of electrons occupying them. For the more stable outer Fe_2, more electrons are on the d_{xy} state (2.72) while less on the $d_{x^2-y^2}$ state (1.95), versus less on the d_{xy} state (2.17) and more on the $d_{x^2-y^2}$ state (2.51) for the inner Fe_2. This indicates that more electrons transfer from the $d_{x^2-y^2}$ state to the d_{xy} state in the bonding of Fe with the outer CNT surface, which enhances their interaction. On the contrary, more electrons stay on the $d_{x^2-y^2}$ state (2.51) of the inner adsorbed Fe_2, which favors the Fe−Fe interaction. As can be seen in Table 1, the Fe−Fe bond length (2.10 Å) is shorter than that of the outer Fe_2 (2.15 Å).

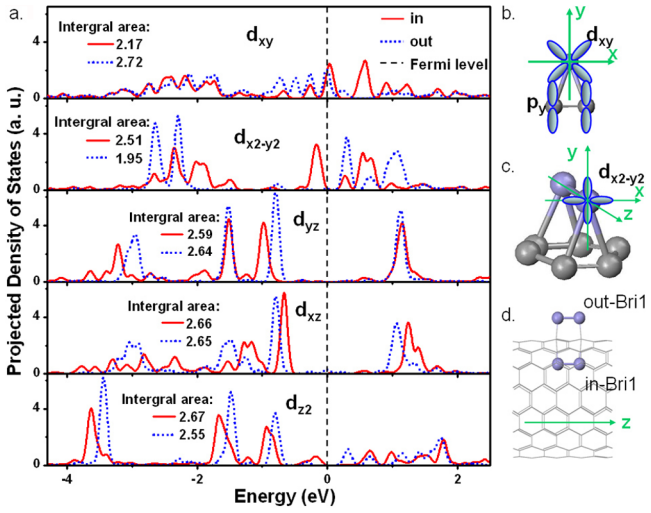

Figure 4. (a) Projected density of 3d states of Fe_2 on the bridge-2 site of a CNT. The integration is conducted over the part below the Fermi level. Configurations of the (b) d_{xy} orbital of Fe_2 and p_y orbital of C and (c) $d_{x^2-y^2}$ orbital of Fe_2. (d) Structures of inner and outer adsorbed Fe_2.

Fewer electrons on the d_{xy} state (2.17 e^-) of the inner Fe_2 lead to relatively weaker bonding with the p_y of C.

The bonding difference can also be seen from the difference in charge density. As shown in Figure 5h, there is an apparent increase of electrons with the shape characteristic of the d_{xy} orbital of the outer Fe_2, whereas this characteristic is unconspicuous for the inner Fe_2 (Figure 5d). In the bonding area between Fe and C the electron-enriched part is apparently larger for the outer case than the inner case, as marked with circles in Figure 5c,g. These electronic analyses rationalize nicely the stronger binding of various iron aggregates on the outer surface than that of the inner one.

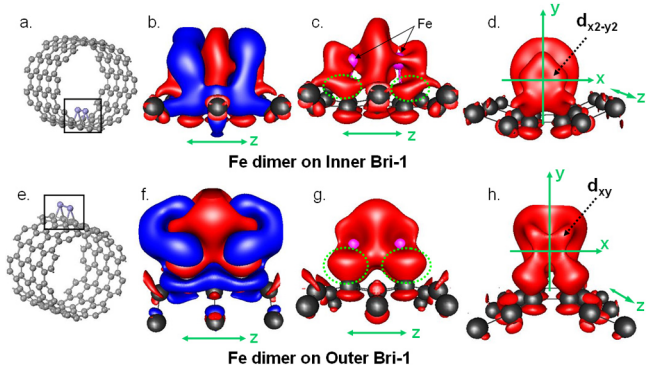

Figure 5. Difference in charge density of Fe_2 adsorbed on the inner and outer bridge-1 sites of a CNT, which is conducted by $\rho_{Fe_2/CNT}-\rho_{CNT}-\rho_{Fe_2}$, where $\rho_{Fe_2/CNT}$, ρ_{CNT}, and ρ_{Fe_2} are the total charge densities of Fe_2/CNT, a pristine CNT, and an isolated Fe_2, respectively: (a, e) structure; (b, f) differential charge density with the blue and red areas denoting decreased and increased charge, respectively; (c, g) only the charge-increased area; (d, h) side views of (c) and (g) along the tube axis. The *x*, *y*, and *z* axes are the Cartesian coordinates of the supercell.

3.3. Curvature-Induced Different Electronic Structures of the Inner and Outer Surfaces. As analyzed in section 3.1, the adsorption of the various iron species on the outer CNT

dx.doi.org/10.1021/jp302311r | J. Phys. Chem. C 2012, 116, 16461−16466

surface is energetically more favored than that on the inner surface. Similar results were reported for Co and Ni atoms and dimers adsorbed on a (4, 4) SWCNT.[11] The frontier orbitals play an important role in the chemical interaction between substances.[24−26] To further understand the origin of such a difference, in particular the influence of the curvature, we studied the electronic structure of the CNT by looking at the distribution of electrons on the highest occupied molecular orbital (HOMO) and lowest unoccupied molecular orbital (LUMO) of (6,6), (8,8), and (10,10) SWCNTs.

When graphene is rolled up to form a tube, the deformation of π bonding causes electron transfer from the crowded concave side to the convex side, inducing a different electron distribution inside and outside the CNT.[27] The data in Table 3

Table 3. Electron Distributions inside and outside the CNTs[a]

SWCNT	in[b]	out[b]	difference	percentage[c]
(6,6)	1.91	2.09	0.18	4.5
(8,8)	1.93	2.07	0.14	3.5
(10,10)	1.95	2.05	0.10	2.5

[a]Only the L electrons (2s + 2p). [b]Electrons per carbon atom, calculated by integrating the amount of inside and outside electrons divided by the tube wall. [c]The percentage is defined by the value of the difference divided by 4 (number of valence electrons of C).

show that there is an apparent quantity disparity between the inner and outer electrons: 0.18, 0.14, and 0.10 more electrons reside on the outer than on the inner surface of (6, 6), (8, 8), and (10, 10) SWCNTs, respectively, which account for 4.5%, 3.5%, and 2.5% of the total number of valence electrons. This is consistent with the previous finding by Haddon.[28] Although this inside−outside difference becomes smaller with increased tube diameter (decreased curvature), the different quantities of inner and outer electrons do affect the bonding strength of iron species with the CNT.

We further look into the properties of the HOMO and LUMO of CNTs. Distributions of one and two electrons filling the HOMO and LUMO of (6, 6), (8, 8), and (10, 10) SWCNTs are investigated.[29] As listed in Table 4, for both frontier orbitals more electrons are distributed on the outside of the tube. This indicates that the frontier orbitals of the CNT are mainly located outside the CNT, as demonstrated by the scheme in Figure 6. Moreover, this difference is remarkably large, accounting for 63% (averaged), 52%, and 46% of frontier orbital electrons for (6, 6), (8, 8), and (10, 10) SWCNTs, respectively. More electron-enriched frontier orbitals on the outer CNT surface may favor the formation of stronger bonding with iron species, as demonstrated above. Though the spatial distribution of the frontier orbitals on the outer surface decreases with an increase of the diameter, it remains significantly higher even for the (10,10) SWCNT with a diameter of 13.6 Å .

4. CONCLUSION

We have chosen a one-dimensional Fe nanowire and FeO nanowire in addition to an Fe atom and dimer as probes to study the interactions of a transition metal with the interior and exterior CNT surfaces. The results show that all these Fe species bond stronger with the outer CNT wall than with the inner one. Analysis of the electronic structure of the CNT indicates that more electrons are distributed on the exterior

Table 4. Electron Distributions on the Inside and Outside Parts of the HOMO and LUMO of CNT

SWCNT[a]	orbital[b]	in[c]	out[c]	difference	percentage[d]
(6, 6)	HOMO ($2e^-$)	0.37	1.63	1.26	63
	HOMO ($1e^-$)	0.20	0.80	0.60	60
	LUMO ($1e^-$)	0.17	0.83	0.66	66
	LUMO ($2e^-$)	0.37	1.63	1.26	63
(8, 8)	HOMO ($2e^-$)	0.47	1.53	1.06	53
	HOMO ($1e^-$)	0.24	0.76	0.52	52
	LUMO ($1e^-$)	0.24	0.76	0.52	52
	LUMO ($2e^-$)	0.48	1.52	1.04	52
(10, 10)	HOMO ($2e^-$)	0.54	1.46	0.92	46
	HOMO ($1e^-$)	0.27	0.73	0.46	46
	LUMO ($1e^-$)	0.27	0.73	0.46	46
	LUMO ($2e^-$)	0.54	1.46	0.92	46

[a]The supercells of (6, 6), (8, 8), and (10, 10) SWCNTs consist of five, four, and three unit cells of the bare tube in the *c* direction so that they have basically the same number of C atoms, i.e., 120 C atoms in the (6, 6) SWCNT, 128 in the (8, 8) SWCNT, and 120 in the (10, 10) SWCNT. [b]The number of electrons filling the frontier orbitals is given in parentheses. [c]Electrons per unit cell. [d]The percentage is defined by the value of the difference divided by the sum of "in" and "out".

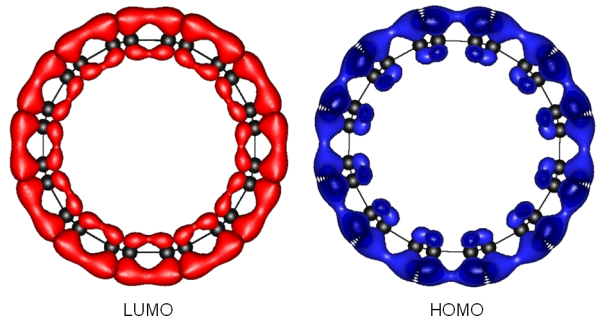

Figure 6. Electronic density distribution of the LUMO and HOMO of the (6, 6) SWCNT.

surface of the CNT. Furthermore, it is demonstrated that the frontier orbitals are mostly located on the outer CNT surface. The more electron-enriched frontier orbitals on the outer wall are expected to be responsible for the stronger bonding of iron species with the outside surface than with the inside. This inside and outside dependence of the bonding strength of iron species may influence their chemical reactivities upon interaction with gas molecules.

AUTHOR INFORMATION

Notes

The authors declare no competing financial interest.

ACKNOWLEDGMENTS

We acknowledge the financial support from the Natural Science Foundation of China (Grants 11079005 and 21033009) and the Ministry of Science and Technology of China (Grant 2011CBA00503).

REFERENCES

(1) Hamada, N.; Sawada, S.; Oshiyama, A. *Phys. Rev. B* **1992**, *68*, 1579.

(2) Blasé, X.; Benedict, L. X.; Shirley, E. L.; Louie, S. G. *Phys. Rev. Lett.* **1994**, *72*, 1878−1881.

(3) Chen, W.; Pan, X. L.; Willinger, M.-G.; Su, D. S.; Bao, X. H. *J. Am. Chem. Soc.* **2006**, *128*, 3136.
(4) Chen, W.; Pan, X. L.; Bao, X. H. *J. Am. Chem. Soc.* **2007**, *129*, 7421.
(5) Chen, W.; Fan, Z. L.; Pan, X. L.; Bao, X. H. *J. Am. Chem. Soc.* **2008**, *130*, 9414.
(6) Pan, X. L.; Fan, Z. L.; Chen, W.; Ding, Y. J.; Luo, H. Y.; Bao, X. H. *Nat. Mater.* **2007**, *6*, 507.
(7) Guo, S. J.; Pan, X. L.; Gao, H. L.; Yang, Z. Q.; Zhao, J. J.; Bao, X. H. *Chem. Eur. J.* **2010**, *16*, 5379.
(8) Chen, Z. J.; Guan, Z. H.; Li, M. R.; Yang, Q. H.; Li, C. *Angew. Chem. Int. Ed.* **2011**, *50*, 4913.
(9) Guan, J.; Pan, X. L.; Liu, X.; Bao, X. H. *J. Phys. Chem. C* **2009**, *113*, 21687.
(10) Vo, T.; Wu, Y. D.; Car, R.; Robert, M. *J. Phys. Chem. C* **2008**, *112*, 8400.
(11) Yagi, Y.; Briere, T. M.; Sluiter, M. H. F.; Kumar, V.; Farajian, A. A.; Kawazoe, Y. *Phys. Rev. B* **2004**, *69*, 075414.
(12) Fagan, S. B.; Mota, R. *Phys. Rev. B* **2003**, *67*, 205414.
(13) Menon, M.; Andriotis, A. N.; Froudakis, G. E. *Chem. Phys. Lett.* **2000**, *320*, 425.
(14) Blochl, P. E. *Phys. Rev. B* **1994**, *50*, 17953.
(15) Kresse, G.; Joubert, D. *Phys. Rev. B* **1999**, *59*, 1758.
(16) Kresse, G.; Hafner, J. *Phys. Rev. B* **1993**, *47*, 558.
(17) Kresse, G.; Hafner, J. *Phys. Rev. B* **1993**, *48*, 13115.
(18) Kresse, G.; Furthmuller, J. *Phys. Rev. B* **1996**, *54*, 11169.
(19) Perdew, J. P.; Chevary, J. A.; Vosko, S. H.; Jackson, K. A.; Pederson, M. R.; Singh, D. J.; Fiolhais, C. *Phys. Rev. B* **1992**, *46*, 6671.
(20) Monkhorst, H. J.; Pack, J. D. *Phys. Rev. B* **1976**, *13*, 5188.
(21) Yuan, S. J.; Kong, Y.; Wen, F. S.; Li, F. S. *Comput. Mater. Sci.* **2008**, *42*, 83.
(22) Sun, Y.; Yang, X. B.; Ni, J. *Phys. Rev. B* **2007**, *76*, 035407.
(23) Kholmanov, I. N.; Gavioli, L.; Fanetti, M.; Casella, M.; Cepek, C.; Mattevi, C.; Sancrotti, M. *Surf. Sci.* **2007**, *601*, 188.
(24) Fukui, K.; Inagaki, S. *J. Am. Chem. Soc.* **1975**, *97*, 4445.
(25) Fukui, K.; Yonezawa, T.; Nagata, C.; Shingu, H. *J. Chem. Phys.* **1954**, *22*, 1433.
(26) Fukui, K.; Yonezawa, T.; Nagata, C. *J. Chem. Phys.* **1957**, *27*, 1247.
(27) Ugarte, D.; Chatelain, A.; Heer, W. A. *Science* **1996**, *274*, 1897.
(28) Haddon, R. C. *Science* **1993**, *261*, 1545.
(29) The electron distributions on the HOMO and LUMO are calculated by $\rho_0 - \rho_+$ and $\rho_- - \rho_0$, respectively, where ρ_0, ρ_+, and ρ_- are the fully optimized total charge densities of a neutral CNT, a CNT with one and two electrons removed from the primitive cell, and a CNT with one and two electrons added to the primitive cell, respectively.